Magnetic properties of $CeNi_{0.84}Sn_2$ studied by magnetization and neutron diffraction



1996 J. Phys.: Condens. Matter 8 8635

(http://iopscience.iop.org/0953-8984/8/44/014)

J. Phys.: Condens. Matter **8** (1996) 8635–8651. Printed in the UK

# Magnetic properties of $CeNi_{0.84}Sn_2$ studied by magnetization and neutron diffraction

P Schobinger-Papamantellos†, J Rodríguez-Carvajal‡, K Prokes§ and K H J Buschow§

† Laboratorium für Kristallographie, ETHZ, CH-8092 Zürich, Switzerland

‡ Laboratoire Léon Brillouin (CEA-CNRS), Centre d'Etudes de Saclay 91191, Gif-sur-Yvette, France

§ Van der Waals-Zeeman Institute, Universiteit Amsterdam, Valckeniersstraat 65, 1018 XE Amsterdam, The Netherlands

Received 24 June 1996

**Abstract.** The magnetic properties of the compound $CeNiSn_2$ were studied by magnetization measurements and neutron diffraction. The refinement of the nuclear structure shows that this compound is slightly Ni-deficient, the corresponding formula being $CeNi_{0.840(4)}Sn_2$. At 1.5 K two coexisting magnetic phases were observed in equal amounts. One of these is ferromagnetic $\boldsymbol{q}_1 = 0$ with $T_C = 3$ K. The other phase is an antiferromagnetic modulated phase (antiphase domain type with two amplitudes) with $T_N = 4.0$ K. Its magnetic ordering can be described in terms of two propagation vectors $\boldsymbol{q}_2 = (010)$ ($C_P$ magnetic lattice) and $\boldsymbol{q}_3 = \frac{1}{3}\boldsymbol{b}^*$. The ordered magnetic moment value at 1.5 K in both phases is $2.0\mu_B$ per Ce atom and points in the same direction along $\boldsymbol{c}$. Above 2 K the wavevector $\boldsymbol{q}_3$ becomes incommensurate with the crystal lattice. The observation of two magnetic phases is attributed to the occurrence of concentration fluctuations associated with the Ni deficiency.

## 1. Introduction

$CeNiSn_2$ crystallizes with the $CeNiSi_2$ type of structure [1–2] (*Cmcm* space group, $a = 0.4485$ nm, $b = 1.774$ nm, $c = 0.4513$ nm, $Z = 4$). According to Skolozdra and Komarovskaya [2] $CeNiSn_2$ forms a range of solid solutions characterized by different degrees of Ni deficiency. It is still an open question whether a compound having the stoichiometric composition really exists. Francois *et al* [3] reported that the upper limit of $x$ in $CeNi_xSn_2$ is 0.74. Investigations of the microstructure of several samples of different composition by means of x-ray methods and electron probe micro-analysis (EPMA) have indicated a higher value for the upper limit of $x$, but still below $x = 1$ [4]. Magnetic properties have been reported for apparently stoichiometric $CeNiSn_2$ which orders antiferromagnetically below $T_N^I = 3.9$ K [2, 5] ($\theta_p = 5$ K and $\mu_{eff} = 2.43\mu_B$). On the basis of specific heat and magnetic susceptibility measurements [5] $CeNiSn_2$ undergoes at 2.6 K a second magnetic phase transition but its Néel temperature is supposed to lie at slightly higher temperatures ($T_N^{II} = 3.2$ K) similarly to the isomorphic $CeNiGe_2$ compound. From plots of unit cell volumes versus atomic number of the lanthanides for the $RNiGe_2$ and $RNiSn_2$ series both Ce compounds show no anomaly indicating a valence fluctuation. The present authors have reported recently on the magnetic ordering of the $CeNiGe_2$ compound on the basis of neutron powder data [6]. The 1.5 K neutron data of $CeNiGe_2$ have shown

0953-8984/96/448635+17$19.50  

the presence of a single magnetic peak, situated in a general reciprocal lattice position which did not allow a complete data analysis. It is of interest in the same context to study the magnetic ordering of $CeNiSn_2$. We will report on magnetic measurements and neutron diffraction experiments on a sample of nominal composition $CeNiSn_{2.1}$, the results of which indicate the coexistence of various types of magnetic ordering.

## 2. Experimental

A sample of the nominal composition $CeNiSn_{2.1}$ was prepared by arc melting from starting elements of at least 99.9% purity. The sample was wrapped in Ta foil and annealed in an evacuated silica tube at 800 °C for three weeks. The excess Sn was chosen in order to compensate for Sn losses during arc melting (Skololozdra and Komarovskaya report [2a] the existence of defect structures both at the Ni and at the $Sn_1$ sites).

Four sets of neutron diffraction data at various temperatures in the range 1.8–293 K and various wavelengths were collected and evaluated by the program Fullprof [7]. Two sets ($\lambda = 0.1704$ and 0.2337 nm) were collected at the Reactor Saphir in Würenlingen, on the DMC (double-axis multicounter system, high-intensity mode) for $T = 1.5$, 3.3 and 10 K and on the double-axis diffractometer P2Ax for 1.5–8.0 K respectively. The step increment in $2\theta$ for both data sets was 0.2°. The other two sets of neutron data were collected at the facilities of the Orphée reactor (LLB-Saclay), using the G4.2 double-axis diffractometer ($\lambda = 0.5995$ nm (1.5–8.0 K) and $\lambda = 0.199\,843$ nm (293 K, with high-resolution mode in the range $2\theta = 1$–155°)). The step increments in $2\theta$ were 0.1° and 0.05° respectively. In view of the expected low value of the Ce moment, neutron diffraction measurements were performed on a large powder sample of nominal composition $CeNiSn_{2.1}$, using a vanadium sample holder of 15 mm diameter. Magnetic measurements were performed on a SQUID magnetometer in the temperature range 1.7–10 K in fields up to 5 T.

## 3. Results and discussion

### *3.1. Magnetic measurements*

Results of magnetic measurements performed in the high-temperature range are shown in figure 1, in which we have plotted the reciprocal susceptibility versus temperature. From the slope of this curve we derive an effective moment of $2.44\mu_B$ per Ce atom, which is close to the value for trivalent Ce. The Curie–Weiss intercept is very small and equal to $\theta_p = -4.8$ K.

Results obtained in the low-temperature range are shown in figure 2. They show that antiferromagnetic ordering occurs close to 4 K, with a second magnetic transition below about 3 K. This is more clearly seen in the temperature-dependence of the AC susceptibility shown in figure 3.

The field-dependence of the magnetization for several selected temperatures is shown in figure 4. The low-field part of the magnetic isotherms is shown in more detail in figure 5. These results show that the antiferromagnetic ordering present at around 4 K can be broken in fairly low magnetic fields, which is accompanied by a small hysteresis. At lower temperatures a ferromagnetic contribution to the magnetization develops. It is very small at 2.9 K but has become much larger at 1.75 K. In fact, the magnetic isotherm at 2.9 K can be decomposed into a very small ferromagnetic contribution and a larger antiferromagnetic contribution. The ferromagnetic contribution dominates the isotherm at 1.75 K, possibly obscuring the presence of any antiferromagnetic contribution. It is very likely that the two

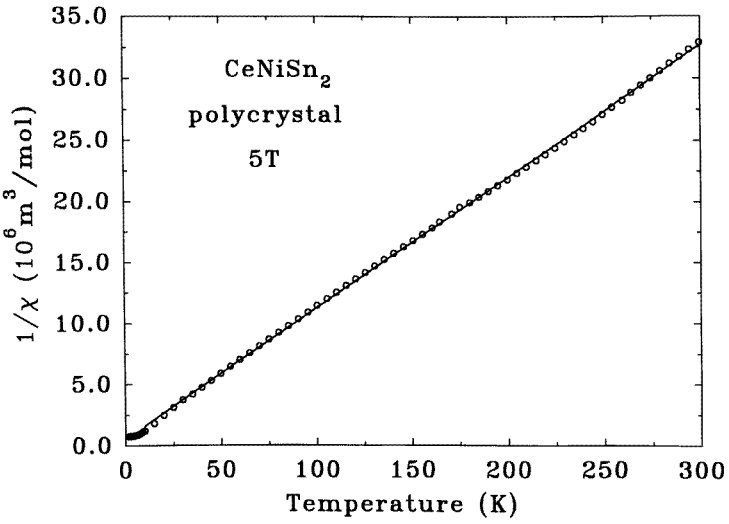


**Figure 1.** The reciprocal susceptibility versus temperature measured in a field of 5 T.

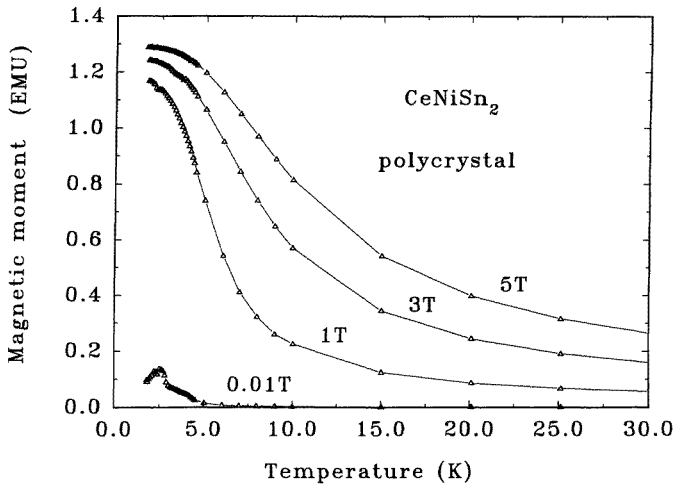


**Figure 2.** The low-temperature magnetization versus temperature for various fields up to 5 T.

contributions are due to two different coexisting magnetic phases. The neutron diffraction data, to be discussed below, have shown that the sample is Ni-deficient, which gives rise to concentration fluctuations associated with the vacancy distribution. Magnetic ordering is therefore not uniform throughout the sample. At 1.5 K roughly half of the sample displays long-range antiferromagnetic ordering. The other half is the ferromagnetic phase. Probably the ferromagnetic phase is present as a spin glass or cluster glass for $T > 3$ K and presumably it is only in the spin glass regions of the sample that the predominant antiferromagnetism can be broken easily at higher temperatures in fairly low fields, as mentioned above. In the other regions the antiferromagnetism remains preserved in all field strengths considered in this investigation.

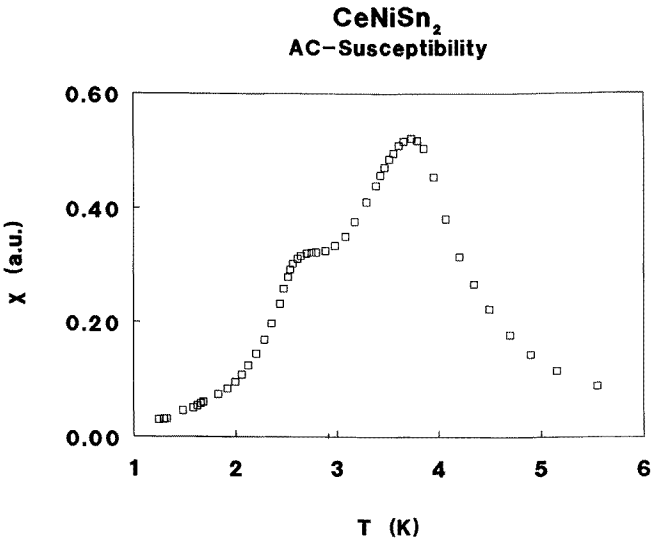


**Figure 3.** The AC susceptibility as a function of temperature.

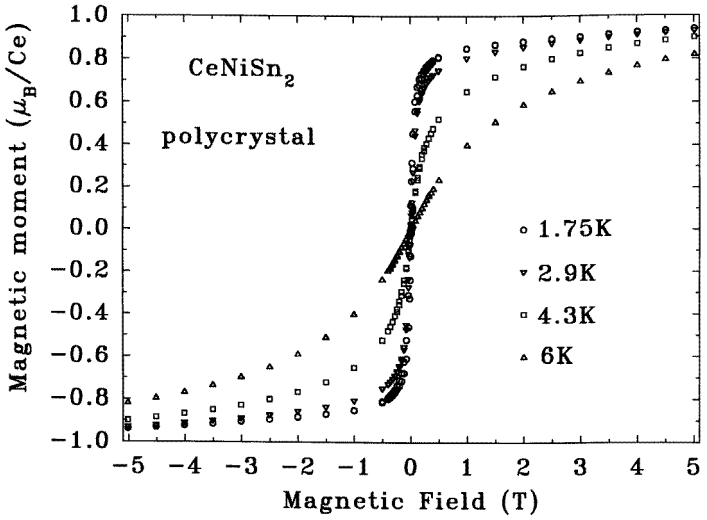


**Figure 4.** The field-dependence of the magnetization for several selected temperatures.

### *3.2. Nuclear structure*

The neutron pattern collected in the paramagnetic state, is shown in figure 6 (top part). The results shown correspond closely to those obtained recently in a detailed determination of the crystal structure of the present compound by means of high-resolution neutron diffraction at room temperature [8]. Results of the latter study and x-ray diffraction made it possible to identify the non-overlapping foreign lines at $2\theta$ angles 49° and 51°, indicated by arrows in figure 6, as belonging to the orthorhombic $Ni_3Sn_2$ [9] compound which was subsequently included in the refinement. The refined parameters given in table 1 confirm the $CeNiSi_2$

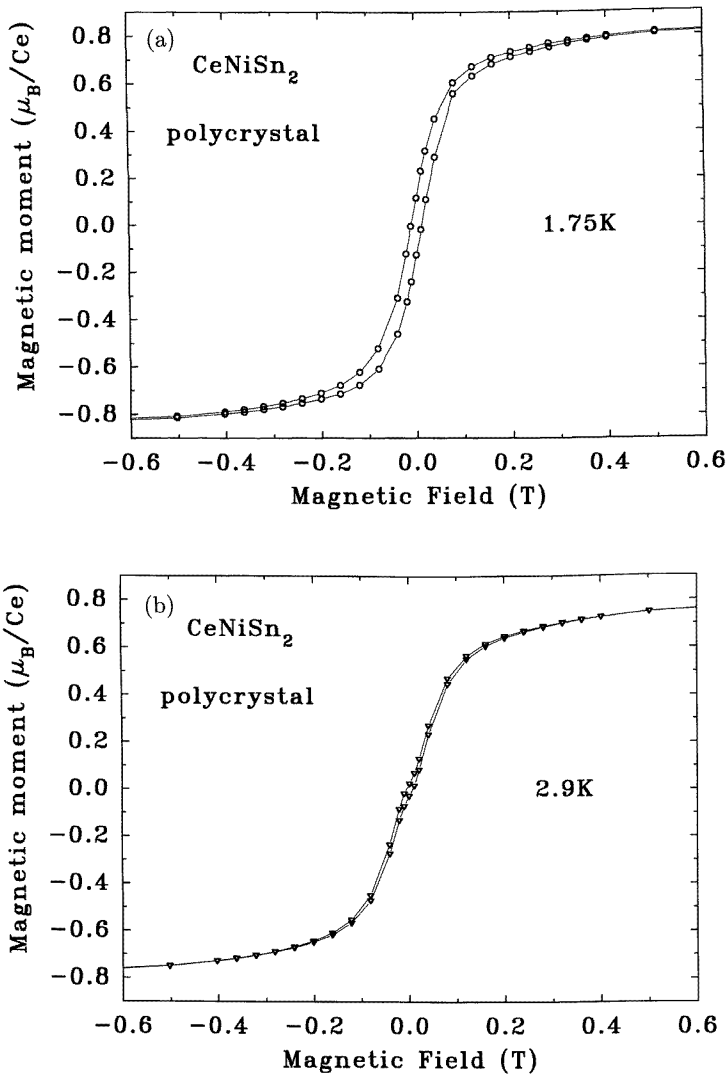


**Figure 5.** The low-field part of the magnetic isotherms of figure 2.

type of structure [1] with a deviation of the Ni occupancy (0.84(1)) from the stoichiometric composition corresponding to the formula $CeNi_{0.84}Sn_2$. The qualitative analysis yields 4.3 wt.% of the $Ni_3Sn_2$ phase. Although the low value of the nuclear reliability factor (4.5%) presents strong evidence in favour of the reported off-stoichiometry, we found high $\chi^2$ values ($> 50$). Apparently these are due to the long counting time applied in the present investigation since the high-resolution neutron diffraction study of the same sample led to much lower values ($\chi^2 = 2$). The enhancement of the nuclear reflections $\{200, 002\}$ and $\{202\}$ visible in the difference diagram at $2\theta$ values $45^\circ$, $65^\circ$ and $68.5^\circ$ was shown to be due to some preferential orientation of the powder particles [8], which is probably associated with their plate-like shape. From the results described above and from the results of the high-resolution neutron diffraction study described elsewhere [8], we can conclude that the

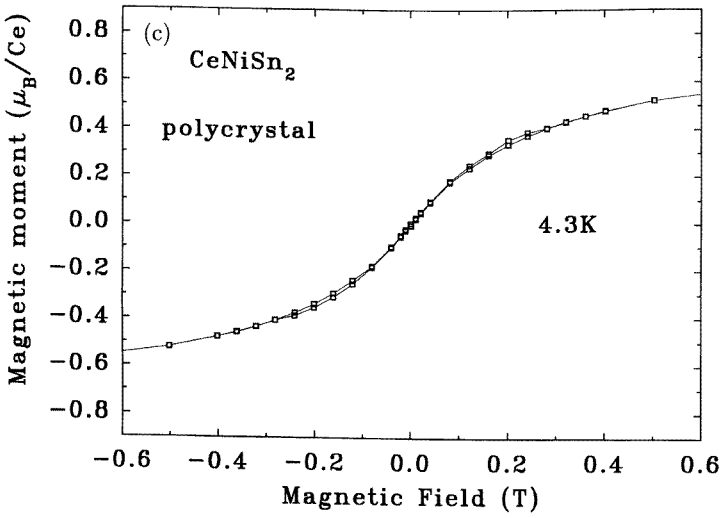


**Figure 5.** (Continued)

$CeNiSi_2$-type compound is present in the paramagnetic regime as a single crystallographic phase. However, the off-stoichiometry associated with the formula $CeNi_{0.84}Sn_2$ implies the presence of concentration fluctuations. As will be shown in the following sections, the magnetically ordered regime is not characterized as a single magnetic phase, regions of different Ni or vacancy concentration leading to different magnetic ordering phenomena.

### *3.3. The uni-axial ferromagnetic phase*

The 1.5 K neutron diffraction pattern in the magnetically ordered state (see figure 6, bottom part) shows no visible changes compared with that obtained in the paramagnetic state at 10 K because the very weak magnetic contributions occur at reciprocal lattice positions of the chemical cell. The only well-resolved change, visible from the enhancement of the (040)/(110) reflections, is shown in figure 7 (top part) on a larger scale. Anticipating the results of the complete data analysis given below, it turns out that even the intensities of these two peaks are composed of five contributing magnetic reflections, indicated by bars at the bottom of the figure part. The deconvoluted peaks are list in table 2.

The relative intensities of the first two observed magnetic reflections, (020) and (040, 110) as shown in the difference diagram figure 8, suggest that $\boldsymbol{b}$ cannot be the easy axis of magnetization and that the intensity enhancement is associated with ferromagnetic contributions. This can be disclosed from the comparison of the observed and calculated intensity ratio $\boldsymbol{I}_{o(020)}/\boldsymbol{I}_{o(040)}$. The calculated intensity ratio resulting from contributions of only the real part of the structure factor (ferromagnetic mode F(++++)) is 0.272, whereas the ratio resulting from the imaginary part (antiferromagnetic mode G(+ − +−)) is 17.93. The former value compares more favourably with the observations $\boldsymbol{I}_{o(020)}/\boldsymbol{I}_{o(040)} \ll 1$. The signs of the F and G modes refer to the moment orientation of the Ce atoms at the 4(c) site: $\boldsymbol{r}_1 = (0, y, \frac{1}{4})$, $\boldsymbol{r}_2 = (0, -y, \frac{3}{4})$, $\boldsymbol{r}_3 = (\frac{1}{2}, \frac{1}{2} + y, \frac{1}{4})$, $\boldsymbol{r}_4 = (\frac{1}{2}, \frac{1}{2} - y, \frac{3}{4})$.

The refinement of the entire 1.5 K neutron pattern converges for a $F_z$ ferromagnetic moment arrangement corresponding to the magnetic space group $Cm'c'm(Sh(^{462}_{63}))$ [10, 11] which allows for the 4(c) symmetry position only a $F_z$ contribution. Apparently the axis of

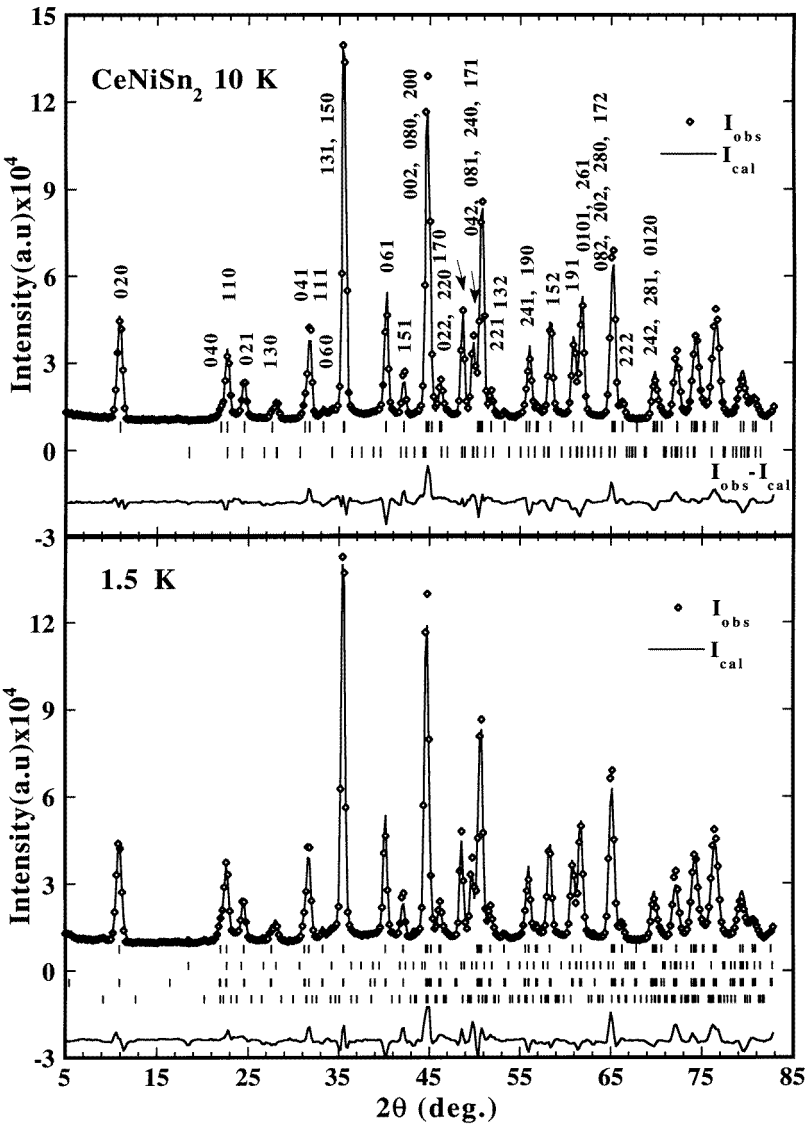


**Figure 6.** Observed and calculated neutron intensities of a sample of nominal composition $CeNiSn_2$ in the paramagnetic state at 10 K (top) and in the magnetically ordered state at 1.5 K. The arrows in the 10 K data indicate the strongest nuclear reflections of $Ni_3Sn_2$. The refined sample composition is $CeNi_{0.84}Sn_2$.

easy magnetization corresponds to the shortest axis ***c***, as already found for some isomorphic compounds of the $RM_xSi_2$ and $RM_xGe_2$ [6, 12] formula. The ordered moment value $(2.1(2)\mu_B)$ for Ce is very close to the full moment value $(gJ\mu_B = 2.14\mu_B)$ of the $Ce^{3+}$ ion, as also suggested in [5].

This result is, however, in contradiction to the magnetic measurements reported in section 3.1, showing a much smaller magnetic moment and predominant antiferromagnetism. Therefore we performed alternatively a refinement based on the difference diagram (1.5–10)K obtained by subtracting from the magnetically ordered data the nuclear contributions,

**Table 1.** Refined structural parameters of the $CeNi_{0.84}Sn_2$ compound in the ferromagnetic paramagnetic state at 10 K and in the magnetically ordered state at 1.5 K. $oc_{Ni}$ is the occupancy of Ni site $\mu_z$ is the ferromagnetic moment value $F_z$ (set I, $\boldsymbol{q}_1 = 0$). $\mu_{(2)} = \mu_{x/z}$ is the antiferromagnetic moment value ($C_x$ or $C_z$) (set II, $\boldsymbol{q}_2 = (010)$). $\mu_{(3)}$ is the antiferromagnetic moment value (Fourier components) giving rise to the transversal amplitude-modulated structure along $c$ (set III, $\boldsymbol{q}_3 = \frac{1}{3}\boldsymbol{b}^*$ or $\boldsymbol{q}_3 = (0q_y0)$). $m_\alpha$ and $m_\beta$ are the moment values in the calculation in the $(\boldsymbol{a}, 3\boldsymbol{b}, \boldsymbol{c})$ cell (column 5).

| | Temperature | | | |
|---|---|---|---|---|
| Parameter | 10 K | 1.5 K(inc) | 1.5-10 K(mod) | 1.5–10 K($\boldsymbol{a}$, 3$\boldsymbol{b}$, $\boldsymbol{c}$) |
| $y_{Ce}$ | 0.1063(5) | 0.1060(5) | 0.1062 | 0.106 |
| $y_{Ni}$ | 0.3169(3) | 0.3168(3) | | |
| $oc_{Ni}$ | 0.84(1) | 0.84(1) | | |
| $y_{Sn(1)}$ | 0.4505(4) | 0.4508(4) | | |
| $y_{Sn(2)}$ | 0.7462(4) | 0.7461(4) | | |
| $\mu_z[\mu_B]$ (set I) | | 1.13(16) | 1.38(3) | 1.38(3) |
| $\mu_{(2)}[\mu_B]$ (set II) | | 0.15(11) | 0.29(1) | |
| $\mu_{(3)}[\mu_B]$ (set III) | | 2.02(14) | | 169(3) |
| $m_\alpha[\mu_B]$, $m_\beta[\mu_B]$ | | | | 1.40(4), 1.13(2) |
| $q_{3y}$ (r.l.u) | | 0.29(1) | 0.333(3) | |
| $a$ (nm) | 0.44675(8) | 0.44673(8) | 0.44672 | 0.466675 |
| $b$ (nm) | 1.7869(3) | 1.7868(4) | 1.78666 | 5.35998 |
| $c$ (nm) | 0.44876(8) | 0.44872(9) | 0.44877 | 0.44877 |
| $B_{of}$ (nm)2 | 0.008(1) | 0.010(1) | 0.0020(6) | 0.0020(6) |
| $R_n$(%), $R_{m1}$(%), $R_{m2}$(%) | 4.5,–,– | 5.78, 11.0, 27 | –, 19.6, 18.0 | –, 18.7, 19.3 |
| $R_{wp}$(%), $R_{\exp}$(%), $\chi^2$ | 11.3, 1.6, 53 | 13.1, 1.43, 83 | 33, 19.3, 2.9 | 33, 19.3, 3.05 |

see figure 8. This was undertaken in order to avoid an artefact of the refinement that could have arisen by refining large nuclear contributions with overlapping weak magnetic peaks.

### *3.4. The difference diagram (1.5–10)K*

In the difference diagram one may distinguish *three sets* of magnetic peaks (denoted by I, II and III) which indicate the coexistence of different types of ordering. As already stated, one set (I) follows the reflection conditions of the nuclear reflections (denoted by arrows in figure 8) with $h + k = 2n$ of the C cell and corresponds to a ferromagnetic moment arrangement along $\boldsymbol{c}(\boldsymbol{q}_1 = 0)$. The second set (II) corresponds to lattice positions of a cell with the same dimensions as the primitive cell with the wavevector $(\boldsymbol{q}_2 = (010))$ and indicates the presence of a small antiferromagnetic component along $\boldsymbol{a}$ or $\boldsymbol{c}$. The only direct observed line is (010) at $2\theta \simeq 5^\circ$. This indicates a symmetry reduction since, for a C magnetic lattice, the low-symmetry 4(c) position $m2m$ allows only uni-axial arrangements of G$(+-+-)$ or F$(++++)$ type [12]. Only an anti-centred magnetic lattice $C_p$ [10, 11] (with the antitranslation operation $\boldsymbol{t}_C = (\frac{1}{2}, \frac{1}{2}, 0)$) is compatible with the reflection condition $(0k0)$ with $k = 2n + 1$. The modes for the 4(c) position compatible with the $C_p$ lattice are C$(++--)$ or A$(+--+)$.

The best fit was achieved for a ferromagnetic moment component $\mu_z = 1.37(3)\mu_B$ per Ce atom for set (I) and a small $C_x$ (or $C_z$) antiferromagnetic contribution of $0.29(1)\mu_B$ per Ce atom for set (II), as given in tables 1 and 2. A projection of the ferromagnetic structure is shown in figure 9(a). Figure 9(b) shows a possible canting of the ferromagnetic structure when assuming that the observed antiferromagnetic $C_x$ ($C_z$) (set II) and ferromagnetic (set I) modes originate from one and the same structure.

**Table 2.** Some of the observed and calculated integrated neutron magnetic intensities of the compound $CeNi_{0.84}Sn_2$ obtained from the refinement of the difference diagram 1.5 K–10 K in the magnetically ordered state by substracting the 10 K nuclear contributions. The indexing $hkl$ (set I) refers to the commensurate ferromagnetic phase $F_z(++++)$. The indexing $hkl^*$ (set II) refers to a possible antiferromagnetic mode $C_x$ (or $C_z$) $(++--)$. The indexing $hkl+/-$ (set III) refers to the magnetic satellites of the incommensurate phase with wavevector $\boldsymbol{q}_3 = \frac{1}{3}\boldsymbol{b}^*$.

| $hkl$ (I) | $hkl^*$ (II) | $2\theta$ (degrees) | $I_{calc}$ | $I^*_{calc}$ | $I_{obs}$ | $hkl \pm q_3$ (III) | $2\theta$ (degrees) | $I_{calc}$ | $I_{obs}$ |
|---|---|---|---|---|---|---|---|---|---|
| | 010* | 5.467 | | 1087 | 1181 | | | | |
| | | | | | | 020− | 9.117 | 1019 | 1039 |
| 020 | | 10.946 | 515 | | 724 | | | | |
| | | | | | | 020+ | 12.717 | 0 | 42 |
| | 030* | 16.450 | | 33 | 272 | | | | |
| 001 | | 21.888 | 0 | | 0 | 040− | 20.140 | 588 | 491 |
| | 100* | 21.990 | | 100 | 91 | 001± | 21.966 | 0 | 0 |
| 040 | | 21.993 | 1724 | | 1572 | {110}− | 22.300 | 1300 | 1376 |
| | 011* | 22.577 | | 4 | 4 | | | | |
| 110 | | 22.676 | 2508 | | 2742 | {110}+ | 23.196 | 578 | 578 |
| | | | | | | {021}− | 23.755 | 166 | 158 |
| 021 | | 24.533 | 652 | | 698 | 040+ | 23.851 | 645 | 603 |
| | 120* | 24.625 | | 8 | 8 | {021}+ | 25.425 | 304 | 92 |
| | 031* | 27.504 | | 36 | 20 | {130}− | 26.503 | 46 | 0 |
| 130 | | 27.586 | 458 | | 246 | {130}+ | 28.751 | 332 | 296 |
| | 101* | 31.222 | | 0 | 0 | {041}− | 29.915 | 144 | 88 |
| 041 | | 31.224 | 204 | | 182 | 060− | 31.355 | 236 | 225 |
| | 140* | 31.298 | | 72 | 68 | {111}− | 31.445 | 136 | 128 |
| 111 | | 31.722 | 748 | | 696 | {111}+ | 32.105 | 444 | 516 |
| | 121* | 33.179 | | 84 | 56 | {041}+ | 32.594 | 22 | 28 |
| 060 | | 33.252 | 358 | | 250 | {150}− | 34.085 | 602 | 588 |
| 131 | | 35.489 | 1460 | | 1376 | {131}− | 34.632 | 656 | 828 |
| 150 | | 35.556 | 1384 | | 1314 | 060+ | 35.157 | 61 | 65 |
| | | | | | | {131}+ | 36.426 | 408 | 380 |
| | 141* | 38.520 | | 16 | 24 | {150}+ | 37.072 | 408 | 436 |
| | | | | | | {061}− | 38.568 | 106 | 144 |
| 061 | | 40.166 | 424 | | 240 | {151}− | 40.877 | 0 | 0 |
| | 160* | 40.225 | | 20 | 12 | {061}+ | 41.799 | 202 | 250 |
| 151 | | 42.144 | 52 | | 24 | 080− | 42.889 | 26 | 0 |
| | | | | | | {151}+ | 43.465 | 80 | 32 |
| 002 | | 44.631 | 0 | | 0 | {170}− | 43.522 | 22 | 14 |
| 200 | | 44.847 | 399 | | 395 | 002− | 44.672 | 0 | 0 |
| 080 | | 44.853 | 137 | | 134 | 200 | 44.888 | 286 | 276 |
| | 012* | 45.000 | | 11 | 10 | {022}− | 45.652 | 2 | 2 |
| | 071* | 45.166 | | 28 | 24 | {220}− | 45.864 | 56 | 12 |
| | 210* | 45.215 | | 22 | 20 | {022}+ | 46.616 | 0 | 0 |
| 022 | | 46.096 | 2 | | 0 | 080+ | 46.830 | 75 | 29 |
| 220 | | 46.306 | 40 | | 14 | {081}− | 48.650 | 160 | 194 |
| | 230* | 48.082 | | 6 | 12 | {171}− | 49.230 | 264 | 264 |
| 042 | | 50.292 | 94 | | 84 | {042}− | 49.420 | 24 | 26 |
| | | | | | | {240}− | 49.620 | 136 | 105 |
| | | | | | | {112}− | 50.441 | 72 | 64 |
| 201 | | 50.438 | 0 | | 0 | 201− | 50.476 | 16 | 16 |
| 081 | | 50.444 | 304 | | 270 | {112}+ | 50.890 | 36 | 36 |
| 240 | | 50.489 | 458 | | 404 | {042}+ | 51.226 | 44 | 56 |
| 112 | | 50.628 | 144 | | 128 | {221}− | 51.371 | 268 | 344 |
| 171 | | 50.779 | 908 | | 796 | {240}+ | 51.421 | 194 | 250 |
| 221 | | 51.778 | 820 | | 1056 | {221}+ | 52.255 | 324 | 356 |
| | | | | | | {081}+ | 52.260 | 70 | 78 |

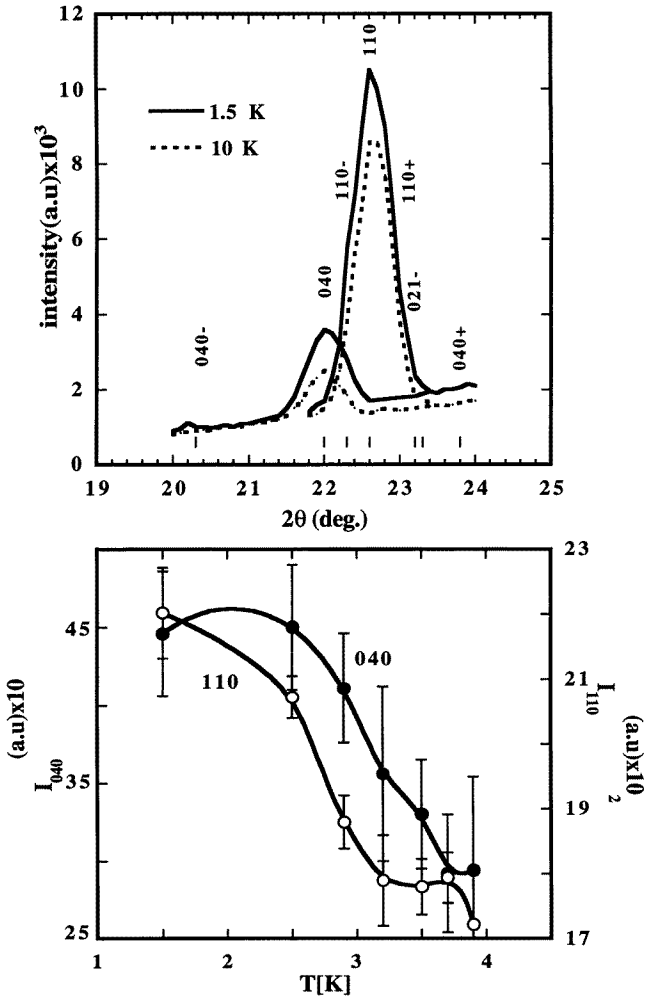


**Figure 7.** The only two resolved reflections with magnetic contributions, {040} and {110}, below and above $T_N = 4.2$ K (top). Also shown is the thermal variation of the ferromagnetic integrated neutron intensities of the reflections {040} and {110} (bottom).

The resulting ferromagnetic uni-axial moment arrangement confirms the $Cm'c'm$ ($Sh(^{462}_{63})$) magnetic space group derived from the analysis of the 1.5 K data. On the other hand, the ordered moment value is more accurate (smaller error) and is reduced by a factor of $\sqrt{2}$ compared with the value resulting from the refinement of the entire 1.5 K data.

However, as will be discussed below, the antiferromagnetic mode (II) when taken parallel to the $\boldsymbol{c}$ axis ($C_z(++--)$ mode) could alternatively be combined with (set III) which pertains to the second magnetic phase also present in the sample. The temperature-dependent measurement (see figure 7 (bottom part)) shows that the ferromagnetic intensity contribution (set I) disappears above $T_C = 3.2$ K, in agreement with the magnetic measurements shown in figure 5.

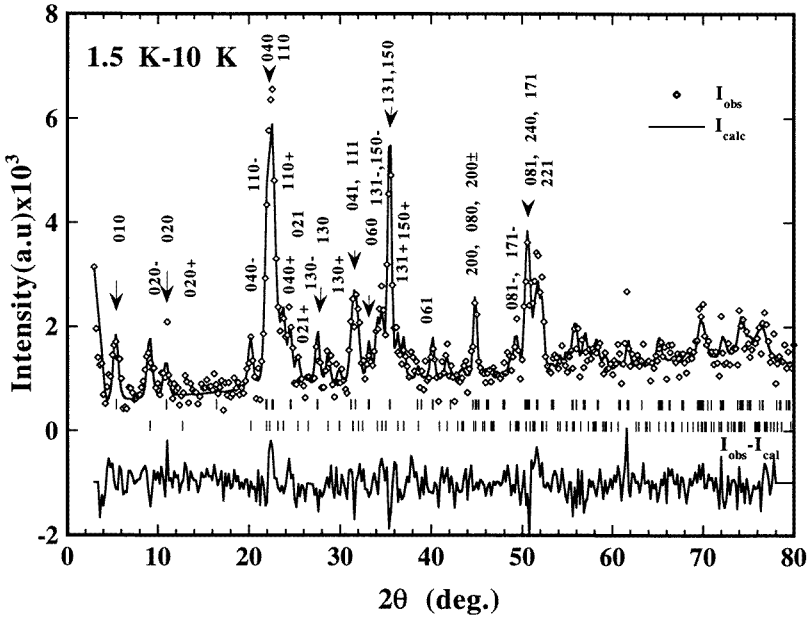


**Figure 8.** Observed and calculated difference diagrams of $CeNi_{0.84}Sn_2$ (1.5–10 K) comprising three sets of magnetic reflections associated with the wavevectors $\boldsymbol{q}_1 = 0$, $\boldsymbol{q}_2 = (010)$ and $\boldsymbol{q}_3 = \frac{1}{3}\boldsymbol{b}^*$.

### *3.5. The modulated magnetic structure $\boldsymbol{q}_3 = (0, q_y, 0)$*

The third set of magnetic reflections (set III) can be directly identified from the presence of weak satellites, $0k0 - \boldsymbol{q}_3$ and $0k0 + \boldsymbol{q}_3$ at either side of the 020 and the 040 reflections. Incidentally the intensity of the 020+ satellite is too small to be detected and the 040+ satellite overlaps with other reflections, see figure 7. On the other hand, since the satellites of the $(0k0)$ reflections are equidistant from the main reflections the wavevector has to be along the $\boldsymbol{b}$ axis. In a powder pattern the $(0k0)\pm$ satellites associated with a wavevector along $\boldsymbol{a}$ or $\boldsymbol{c}$ coincide and appear at larger $2\theta$ angles relative to the main reflection. It has been possible to index these reflections as satellites of the nuclear reflections of the reciprocal $C$ lattice $(\boldsymbol{a}^*, \boldsymbol{b}^*, \boldsymbol{c}^*)$ using a wavevector $\boldsymbol{q}_3 = (0, q_y, 0)$ with $q_y \approx \frac{1}{3}$. We will see that, in spite of the weakness of these reflections, we can establish a model that explains the observed pattern and predicts the existence of an intense $(0, 0, 0) \pm \boldsymbol{q}_3$ satellite. This satellite has been observed using long-wavelength neutrons (see section 3.8). The magnetic 'satellite' reflections appear at points

$$\boldsymbol{Q} = 2\pi(\boldsymbol{H} \pm m\boldsymbol{q}_3) \tag{1}$$

where $\boldsymbol{H}$ is a reciprocal lattice vector of the chemical cell and $m$ an integer. In the Fourier representation of magnetic structures a periodic moment arrangement $\mu_{nj}$ is expressed as the superposition of all observed Fourier coefficients $(\boldsymbol{S}_{qj}, \boldsymbol{S}_{-qj})$ associated with the wavevector(s) $\pm\boldsymbol{q}$ [13]. Thus the full description of a magnetic structure with several wavevectors implies the knowledge of the directions of the magnetic moments for each $\boldsymbol{S}_{qj}$

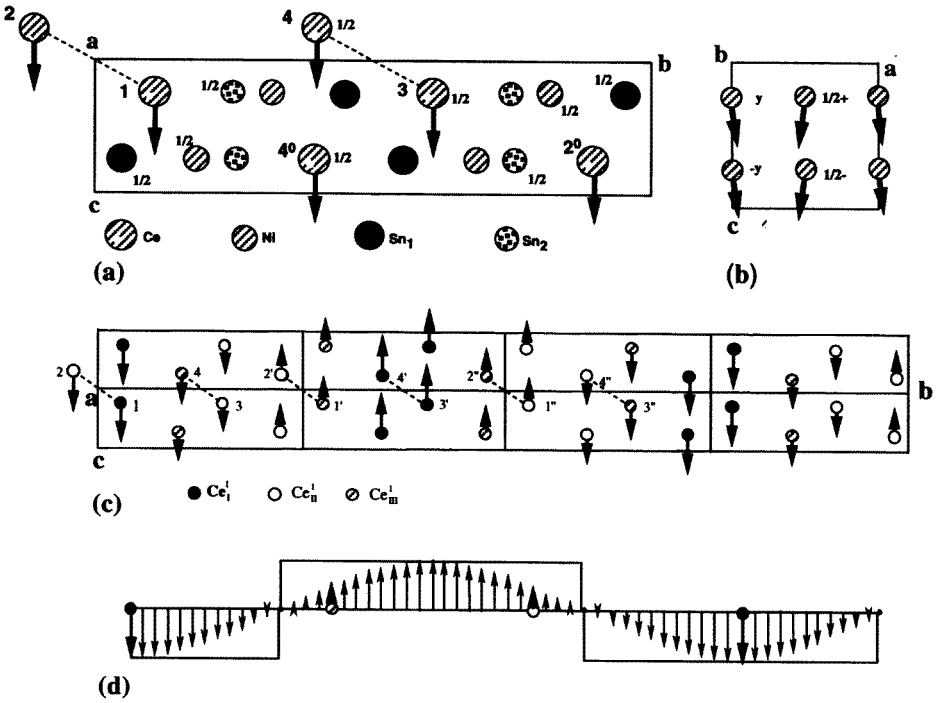


**Figure 9.** A projection of the magnetic structures observed in the neutron data at 1.5 K of $CeNi_{0.84}Sn_2$: (a) the ferromagnetic mode parallel to $c$ in the (100) plane, (b) the ferrimagnetic mode in the (010) plane and, (c) the transversal amplitude-modulated structure with wavevector $\boldsymbol{q}_3 = \frac{1}{3}\boldsymbol{b}^*$ and the square wave with $\boldsymbol{q}_2 = (010)$ and $\boldsymbol{q}_3 = \frac{1}{3}\boldsymbol{b}^*$. Atom labels $j$, $j'$ and $j''$ refer to the parameters defined in the incommensurate description ($Ce_j$, $j = 1$–4) while different patterns ($Ce^1_I$, $Ce^1_{II}$, and $Ce^1_{III}$) were used to show the threefold splitting of the 4c site in the commensurate description.

and the coupling between the various $\boldsymbol{S}_{qj}$ [7]:

$$\boldsymbol{\mu}_{nj} = \sum_{(q)} \boldsymbol{S}_{qj} \exp(-2\pi \boldsymbol{q}\cdot\boldsymbol{R}_n) = \sum_{\{q\}} \boldsymbol{T}_q \exp\{-2\pi\, \mathrm{i}\boldsymbol{q}\cdot\boldsymbol{R}_{nj}\} \tag{2}$$

where $\boldsymbol{R}_{nj}$ is a positional vector of the $j$th atom in the $n$th cell ($\boldsymbol{R}_{nj} = \boldsymbol{R}_n + \boldsymbol{r}_j$).

Since only first-order satellites were observed, we first applied a model with a sine wave incommensurate modulated phase. In such a structure the moment value $\mu_{nj}$ of the $j$th atom in the $n$th cell may be derived from the moment value (Fourier coefficients) in the *zeroth* cell:

$$\boldsymbol{\mu}_{nj} = \sum_{q} S_{qj} \exp(-2\pi \mathrm{i}\boldsymbol{q}\cdot\boldsymbol{R}_n) = \mu_{0j}\cos(2\pi\boldsymbol{q}\cdot\boldsymbol{R}_n + \varphi_j) = \mu_{0j}\boldsymbol{z}\cos(2\pi\boldsymbol{q}\cdot\boldsymbol{R}_n + \varphi_j) \tag{3}$$

where $\boldsymbol{z}$ is a unit vector in the direction of the varying moment component, $\mu_{0j}$ is the amplitude of the sinusoidal variation and $\varphi_j$ is a phase factor of the $j$th atom relative to the origin of the wave, which is usually taken at atom (1). In our case a reasonable assumption is that the four Ce atoms of the same (4c) site have the same wave amplitude $\mu_{0j} = \mu_{(3)}$. From the fact that the magnetic reflections are satellites of only the allowed nuclear reflections $hkl$ with $h + k = 2n$ we can conclude a phase of only $2\pi\boldsymbol{q}\cdot\boldsymbol{t}_C = \pi/3$,

between atoms related by the $C$ translation operation. In fact formula (3) describes the full magnetic structure if centring translations are included in $\boldsymbol{R}_n$, so only the two atoms in a primitive cell, namely with position vectors $\boldsymbol{r}_1 = (0, y, \frac{1}{4})$, and $\boldsymbol{r}_2 = (0, -y, -\frac{1}{4})$, have to be considered. Therefore the parameters to be refined from the neutron magnetic intensities are the amplitude length $\mu_{(3)}$ and the direction $\boldsymbol{z}$ of polarization, the phase angle between the atoms at $\boldsymbol{r}_1$ and $\boldsymbol{r}_2$ and the wavevector length $q_y$.

From the possible models the best fit was obtained for a transversal amplitude-modulated structure with the moments polarized along the $\boldsymbol{c}$ axis as found for the ferromagnetic phase. The refined amplitude value corresponds to $1.69(3)\mu_B$ per Ce atom and the phase is zero.

Within the error limits (we have used restricted resolution for the selected experimental conditions: large sample radius and large step of $0.2^\circ$) the wavevector length can be approximated as a threefold cell enlargement along the $\boldsymbol{b}$ axis $\boldsymbol{q}_3 = (0, \frac{1}{3}, 0)$. The moment arrangement resulting from equation (3) is displayed in figure 9(c). If we note the atoms related to the cell at the origin by translations $\boldsymbol{t}_b$ and $2\boldsymbol{t}_b$ with prime and double prime, the values of the magnetic moments in the triple crystallographic cell are given by the following relations.

For the reference crystallographic cell: $\boldsymbol{R}_n = (0, 0, 0)$ and $\boldsymbol{R}_n = (\frac{1}{2}, \frac{1}{2}, 0)$

$$\mu_j = \mu_{(3)} \qquad \text{for } j = 1, 2$$
$$\mu_j = \mu_{(3)} \cos(\pi/3) = \mu_{(3)}/2 \qquad \text{for } j = 3, 4.$$

For the cell translated by $\boldsymbol{t}_b$: $\boldsymbol{R}_n = (0, 1, 0)$ and $\boldsymbol{R}_n = (\frac{1}{2}, \frac{3}{2}, 0)$

$$\mu_j = \mu_{(3)} \cos(2\pi/3) = -\mu_{(3)}/2 \qquad \text{for } j = 1', 2'$$
$$\mu_j = \mu_{(3)} \cos(3\pi) = -\mu_{(3)}/2 \qquad \text{for } j = 3', 4'.$$

For the cell translated by $2\boldsymbol{t}_b$: $\boldsymbol{R}_n = (0, 2, 0)$ and $\boldsymbol{R}_n = (\frac{1}{2}, \frac{5}{2}, 0)$

$$\mu_j = \mu_{(3)} \cos(4\pi/3) = -\mu_{(3)}/2 \qquad \text{for } j = 1'', 2''$$
$$\mu_j = \mu_{(3)} \cos(5\pi/3) = \mu_{(3)}/2 \qquad \text{for } j = 3'', 4''.$$

Two values of the magnetic moment $m = \mu_{(3)}$ and $m' = \mu_{(3)}/2$ are present in this sinusoidal model. Of course, for a sinusoidal structure there is a global phase that does not affect the magnetic intensities and is arbitrary. The choice of this phase ($\Phi = 0$ for us) will determine the value of the moments in the different cells.

### *3.6. The commensurate approximation ($\boldsymbol{a}$, $3\boldsymbol{b}$, $\boldsymbol{c}$)*

The existence of a commensurate wavevector value $\boldsymbol{q}_3 = \frac{1}{3}\boldsymbol{b}^*$ makes available the possibility of performing the calculations also as if for a commensurate structure with a three times larger cell ($\boldsymbol{a}$, $3\boldsymbol{b}$, $\boldsymbol{c}$), the two methods being equivalent. The cell enlargement $3\boldsymbol{b}$ leads to the space group $Cmcm$ [14] and the 4(c) position splits into three 4(c) positions: $Ce^1_I$ $(0, y/3, \frac{1}{4})$, $Ce^1_{II}$ $(0, (1-y)/3, \frac{3}{4})$, and $Ce^1_{III}$ $(0.5, (0.5-y)/3, \frac{3}{4})$, with $y = 0.106$; see also figure 9(c).

The best fit was obtained for a collinear moment arrangement along $\boldsymbol{c}$ with the $C_z(++--)$ mode. Because of the $C_p$ antitranslation each sub-lattice is antiferromagnetic. The sub-lattices $Ce^1_I$ and $Ce^1_{III}$ are parallel whereas $Ce^1_{II}$ is perpendicular. There are two different ordered moment values: $m_\alpha = \mu_{Ce^1_I} = 1.40(4)\mu_B$ and $m_\beta = -\mu_{Ce^1_{II}} = \mu_{Ce^1_{III}} = -1.13(2)\mu_B$. The magnetic space group is $C_p m'c'm$ or, in the Shubnikov notation, $P_B nma$ ($Sh\ (^{454}_{62})$), [10b, 11].

### *3.7. The squaring up of the modulated magnetic structure*

The two values of the magnetic moments $(m, m')$ in (4) are not the same as the two magnetic moments of the commensurate description because $m_\alpha/m_\beta \neq \frac{1}{2}$ whereas $m/m' = \frac{1}{2}$. This is because the calculation as a commensurate phase with a $C_p$ lattice comprises all $hkl$ observations (with $k = 3n$ and $k = 3n \pm 1$) whereas in the description of a pure sinusoidal modulated structure only first order satellites ($k = 3n \pm 1$) were considered. The two results can be rendered equivalent if one considers a possible deviation from the sinusoidal modulation or a squaring up. Using formula (3) and including the Fourier coefficients of the third harmonic $3\boldsymbol{q}_3$, which is equivalent to the vector addition of the Fourier component $\boldsymbol{S}_{(q2)}$ with a moment amplitude $\mu_{(2)} = 0.29(1)\mu_B$ per Ce of the $C_z(++--)$ mode with $\boldsymbol{q}_2 = (010) = 1\boldsymbol{b}^*$ (see section 3.4), one obtains the full structure description using a phase of $\pi$ between $\boldsymbol{S}_{(q2)}$ and $\boldsymbol{S}_{(q3)}$ (remember that $\mu_{(3)} = 1.69(1)\mu_B$ per Ce):

$$\boldsymbol{M}_{nj} = \sum_q S_{qj} \exp(-2\pi \mathrm{i} \boldsymbol{q} \cdot \boldsymbol{R}_n) = \mu_{(2)} \cos(2\pi \boldsymbol{q}_2 \cdot \boldsymbol{R}_n + \pi) + \mu_{(3)} \cos(2\pi \boldsymbol{q}_3 \cdot \boldsymbol{R}_n) \tag{4}$$

$$\boldsymbol{M}_{nj} = -\boldsymbol{\mu}_{(2)} \cos[2\pi(n + \delta/2)] + \boldsymbol{\mu}_{(3)} \cos[2\pi(n + \delta/2)/3] \tag{5}$$

with $\delta = 0$ for integer translations (atoms 1 and 2) and $\delta = 1$ for centred translations (atoms 3 and 4). Applying formula (4) and taking into account that the common direction of the amplitudes $\mu_{(2)}$ and $\mu_{(3)}$ is $\boldsymbol{z}$, we obtain for $n = 0$

$$M_1 = M_2 = -\mu_{(2)} + \mu_{(3)} = 1.40\mu_B = m_\alpha \tag{6}$$

$$M_3 = M_4 = \mu_{(2)} + \mu_{(3)} = 1.135\mu_B = -m_\beta \tag{7}$$

The reader can verify that the formula (4) gives the same magnetic structure as that described in section 3.6.

The ratio of the amplitudes of the Fourier coefficients $Q = \mu_{(2)}/\mu_{(3)}$ is a measure of the deviation of the structure from the pure sinusoidal model towards an antiphase domain structure in which translationally equivalent atoms have the same moment value but their signs may vary from cell to cell in the direction of the wavevector in a periodic way, namely for $\boldsymbol{q}_3 = \frac{1}{3}\boldsymbol{b}^*$ one obtains the ferrimagnetic chain $\pm(++-++-\cdots)$. However, due to the phase shift $\pi/3$ between atoms related by the $C$ translation the total is antiferromagnetic.

For $\mu_{(2)} = 0$, $Q = 0$, the collinear magnetic structure is a purely sine-wave-modulated structure or an antiphase domain with two amplitudes. For, $Q = (1 - \cos\pi/3)/2 = \frac{1}{4}$ the structure would be a purely antiphase domain type with the moments having the same value but different signs. For any value $0 < Q < \frac{1}{4}$ the collinear modulated structure begins to square up and needs for its description at least two different magnetic moments. The value of $Q$, is in general temperature-dependent and can be directly deduced from the intensity variation with temperature of the (010) reflection and of, for instance, the $000 - \boldsymbol{q}_3$ satellite as will be given below (see figure 10). At 1.5 K $Q = (0.29/1.69) = 0.17$, which indicates that the structure is closer to the antiphase domain type and that the modulated antiferromagnetic structure squares up.

### *3.8. Thermal variation of the wavevector $\boldsymbol{q}_3$ and of the $(000) \pm \boldsymbol{q}_3$, satellite intensity*

The magnetic structure model for the antiferromagnetic part of the sample seems quite complex and is based on weak reflections. However, as stated above, the model predicts a low-$Q$ reflection, the $(0, 0, 0)\pm$ satellite, having much greater intensity than any other magnetic peak. We performed a diffraction experiment using neutrons of wavelength close to 6 Å. The corresponding data confirm nicely the prediction obtained from relatively noisy data and allow a more direct identification of the magnetic satellites because of the higher

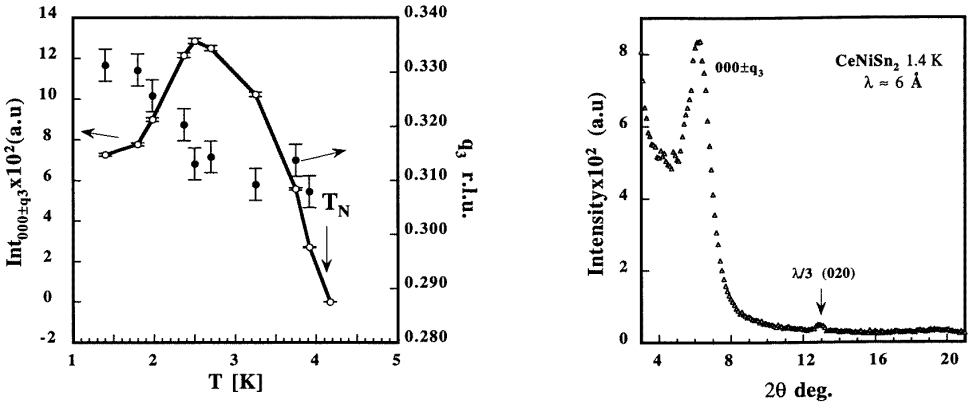


**Figure 10.** (a) The temperature-dependence of the wavevector $\boldsymbol{q}_3 = (0, q_y, 0)$ in r.l.u. Also shown is the temperature-dependence of the integrated neutron intensity of the $000-\boldsymbol{q}_3$ satellite. (b) The zero-point satellite $000 - \boldsymbol{q}_3$ at 1.4 K for $\lambda \approx 6$ Å.

resolution. Due to the allocated beam time only the low $2\theta$ angle (0–65°) data are available to us at present for a full set of temperatures (1.4–10)K. The temperature-dependence of the wavevector length and of the integrated neutron intensity of the zero-point satellite $000 \pm \boldsymbol{q}_3$ magnetic reflection that has become visible at $2\theta \approx 6°$ are displayed in figure 10. These data confirm the 1.5 K refined lock-in value of the wavevector $\boldsymbol{q}_3 = (0, q_y, 0)$ with $q_y = \frac{1}{3}$ but this value is restricted to the low-temperature region $T < 2$ K. Above this temperature the wavevector length decreases continuously with $T$ and the magnetic structure becomes incommensurate with the crystal lattice. The very weak (010) reflection seems also to disappear above the lock-in temperature of about 2 K.

### *3.9. The Ce ordered moment value of the two phases*

Given the fact that the ferromagnetic (set I) and antiferromagnetic (sets II and III) phases result in about to the same refined ordered moment values of about $1.40\mu_B$ per Ce (table 1, column 5), we can assume that the composition $x = 0.84$ is a critical value in the magnetic $(T, x)$ phase diagram of the $CeNi_xSn_2$ system and that the two magnetic phases are present in equal amounts. In order to derive the correct moment value for each of these two phases we have to re-scale the magnetic intensities by taking into account that both phases constitute only half of the sample. After multiplication by $\sqrt{2}$ we find moment values of $2.0\mu_B$ per Ce for each phase. The derived moment value is very close to the free-ion value of $(gJ\mu_B = 2.14\mu_B)$ of the $Ce^{3+}$ ion. The presence of the wavevector $\boldsymbol{q}_3 = \frac{1}{3}\boldsymbol{b}^*$ and of a collinear structure indicate the existence of a strong crystal field anisotropy and the presence of competing interactions, leading to complex ordering mechanisms, as pointed out by Kimura in [15, 16] for the orthorhombic $TbCu_2$ compound, showing specific heat anomalies and a lock-in transition with wavevector $\boldsymbol{q} = \frac{1}{3}\boldsymbol{a}^*$.

It is interesting to compare the Ce moment value derived above for the two phases with the results of the magnetic measurements. Assuming that the contribution of the antiferromagnetic phase to the saturation magnetization can be neglected, we find for the ferromagnetic phase a saturation moment at 1.75 K equal to $2 \times 0.94\mu_B$ per Ce$= 1.9\mu_B$ per Ce (see figure 4). This value is in satisfactory agreement with the neutron data.

## 4. Concluding remarks

In the derivation of complex magnetic moment arrangements from neutron data involving the coexistence of several Fourier coefficients one is always confronted with an ambiguity in the choice of model. This difficulty arises from the fact that the neutron experiment does not provide any information about the phases between Fourier coefficients [13] since they do not contribute to the same set of reflections. So it could be that the structure consists of coexisting domains rather than the Fourier coefficients of the various vectors adding up coherently. To overcome this difficulty one needs further information from other physical properties.

In the present case we are confronted with three sets of Fourier coefficients pertaining to ferromagnetic ordering $F_z$ with $\boldsymbol{q}_1 = 0(h+k=2n)$, to the antiferromagnetic ordering $C_x$ or $C_z(++--)$ with $\boldsymbol{q}_2 = (010)$ and to a modulated antiferromagnetic ordering pertaining to the wavevectors $\pm\boldsymbol{q}_3 = (0, q_y, 0)$. By performing refinements under the simplest assumptions, we derived the conclusion that the examined sample consists of only *two coexisting magnetic phases*.

We cannot completely rule out the possibility that these two phases correspond to two distinct nuclear structures with neighbouring compositions, having within experimental accuracy the same lattice constants and being therefore not distinguishable by diffraction methods. A more likely interpretation of the occurrence of two magnetic phases may be sought in density fluctuations at the Ni site. In this connection we would like to mention the results obtained by Lambert-Andron *et al* [17, 18], who reported the coexistence of ferromagnetic and antiferromagnetic phases even within a single crystal. Also here there is a defect compound ($CeGe_{2-x}$ with $x \approx 0.4$) and the two coexisting phases correspond to different degrees of ordering of the Ge vacancies present in the defect structure.

In fact, strong experimental evidence for the occurrence of a Ni deficiency in the sample investigated by us can be derived from the results discussed in section 3.2. Although such Ni deficiency would follow already from the nominal composition of the sample and the observation of 4.3 wt% of $Ni_3Sn_2$ as impurity phase, we have presented rather direct evidence in the form of the refinement of the nuclear structure that had indicated a Ni site occupancy of only 0.84(1). Exactly the same degree of Ni deficiency was derived from the high-resolution neutron diffraction results [8]. This Ni deficiency means that there are Ni concentration fluctuations and a concomitant distribution in interatomic distances. It is likely that the presence of these concentration fluctuations is the origin of the coexistence of a ferromagnetic phase and a modulated antiferromagnetic (antiphase domain type) phase in the low-temperature range.

It is interesting to compare the results obtained in the course of the present investigation with results obtained on nominally pure $CeNiSn_2$ [5]. In the latter case specific heat measurements and/or magnetic measurements have shown the presence of two-step magnetic orderings. This allows the interesting possibility that the transition at the higher temperature ($T_N^I$) corresponds to a transversally sine-wave-modulated antiferromagnetic ordering $\boldsymbol{q}_3 = (0, q_y, 0)$ whereas the transition at lower temperature ($T_N^{II}$) corresponds to the lock-in transition of the wavevector and the squaring up of the modulated structure (collinear antiphase domain type) described by two wavevectors ($\boldsymbol{q}_3 = \frac{1}{3}\boldsymbol{b}^*$ and $\boldsymbol{q}_2 = 1\boldsymbol{b}^*$ (the $C_P$ lattice)), see section 3.5, because of the entropy term in the free energy.

However, the persistence of the two-step character of the magnetic ordering observed on nominally more deficient $CeNi_xSn_2$ compounds [4] over wide concentration ranges seems rather to be connected to the presence of ferromagnetism at lower temperatures. In all cases two transitions were found, the high-temperature transition corresponding to

antiferromagnetic ordering. In some regions of the sample having a vacancy concentration below (or above) a critical value, the atomic disorder results in a cluster-glass-type magnetic ordering instead of antiferromagnetic ordering. The difference between the various samples would then primarily be a difference in the relative amounts of the regions, giving rise to long-range antiferromagnetic ordering as well as a difference in the nature and size of the cluster glass regions and their distribution. Even when present in relatively small amounts, these latter regions will have a strong influence on the low-temperature magnetization because of the development of ferromagnetic order, as observed by neutron diffraction in the sample investigated by us. Owing to the easy generation of domain walls in such two-phase systems (already in positive field in at least some of the ferromagnetic regions) the hysteresis loops are expected to have a less common shape also in samples having a fairly large amount of the ferromagnetic phase at low-temperatures. Neutron diffraction studies on these nominally more Ni deficient $CeNi_xSn_2$ compounds are planned in the near future.

## Acknowledgment

The authors wish to thank Dr C H Niewenhuys for fruitful discussions.

## References

[1] Bodak O P and Gladyshevskii E I 1970 *Sov. Phys. Crystallogr.* **14** 859
[2] Skolozdra R V and Komarovskaya L (a) 1988 *Izv. Akad. Nauk SSSR Met.* **2** 214 *(Russ. Metall. Met.* **2** 207); (b) 1988 *Phys. Met. Metall.* **65** No3 99
[3] Francois M, Venturini G, Malaman B and Roques B 1990 *J. Less-Common Met.* **160** 197
[4] Lemmens L W F J, Nieuwenhuys G H, Schobinger-Papamantellos P and Buschow K H J 1996 to be published
[5] Pecharsky V K, Gschneidner K A Jr and Miller L L 1991 *Phys. Rev.* B **43** 10 906
[6] Schobinger-Papamantellos P, Krimmel A, Grauel A and Buschow K H J 1993 *J. Magn. Magn. Mater.* **125** 151
[7] Rodríguez-Carvajal J 1993 *Physica* B **192** 55
[8] Schobinger-Papamantellos P, Rodríguez-Carvajal J and Buschow K H J 1996 *J. Alloys Compounds* **240** 85
[9] Fjellvag H and Kjekshus A 1986 *Acta Chem. Scand.* A **40** 23
[10] Bertaut E F (a) 1963 *Magnetism* vol 3, ed G T Rado and H Suhl (New York: Academic) Press, New York, 1963) p 149; (b) 1975 *Ann. Phys.* **9** 93
[11] Koptsik V A 1966 *Shubnikov Groups* (Moscow: Moscow University Press)
[12] Schobinger-Papamantellos P and Buschow K H J 1991 *J. Less-Common Met.* **171** 321
[13] Rossat-Mignod J 1987 *Neutron Scattering* (New York: Academic)
[14] Hahn Th (ed) 1983 *International Tables for Crystallography* (Dordrecht: Reidel)
[15] Kimura I (a) 1985 *J. Magn. Magn. Mater.* **52** 199 (b) 1988 *J. Magn. Magn. Mater.* **76** 191
[16] Iwata N, Kimura T, Shigeoka T and Hashimoto Y 1987 *J. Magn. Magn. Mater.* **70** 279
[17] Lambert-Andron B, Boutarek N, Pierre J and Madar R 1994 *J. Alloys Compounds* **203** 1
[18] Lambert-Andron B, Houssay E, Madar R, Hippert F, Pierre J and Auffret S 1990 *J. Less-Common. Met.* **167** 53